Harnessing molecular excited states with Lanczos chains

2010 J. Phys.: Condens. Matter 22 074204

(http://iopscience.iop.org/0953-8984/22/7/074204)

J. Phys.: Condens. Matter **22** (2010) 074204 (8pp) doi:10.1088/0953-8984/22/7/074204

Harnessing molecular excited states with Lanczos chains

Stefano Baroni[1,2], Ralph Gebauer[2,3], O Barış Malcıoğlu[1], Yousef Saad[4], Paolo Umari[2] and Jiawei Xian[1]

[1] SISSA—Scuola Internazionale Superiore di Studi Avanzati, I-34151 Trieste, Italy
[2] CNR DEMOCRITOS Theory@Elettra Group, c/o Sincrotrone Trieste, Area Science Park, I-34012 Basovizza, Trieste, Italy
[3] The Abdus Salam International Centre for Theoretical Physics, I-34151 Trieste, Italy
[4] Department of Computer Science and Engineering, University of Minnesota, and Minnesota Supercomputing Institute, Minneapolis, MN 55455, USA

Received 23 October 2009, in final form 7 January 2010
Published 3 February 2010
Online at stacks.iop.org/JPhysCM/22/074204

Abstract
The recursion method of Haydock, Heine and Kelly is a powerful tool for calculating diagonal matrix elements of the resolvent of quantum-mechanical Hamiltonian operators by elegantly expressing them in terms of continued fractions. In this paper we extend the recursion method to off-diagonal matrix elements of general (possibly non-Hermitian) operators and apply it to the simulation of molecular optical absorption and photoemission spectra within time-dependent density-functional and many-body perturbation theories, respectively. This method is demonstrated with a couple of applications to the optical absorption and photoemission spectra of the caffeine molecule.

(Some figures in this article are in colour only in the electronic version)

Density-functional theory (DFT) [1, 2] is currently considered the state of the art in the simulation of materials at the atomic (nano-) scale [3], based on electronic-structure theory [4]. Although the scope of DFT is limited by construction to the electronic ground state, many material properties can be accurately and—with the aid of the powerful algorithms and computers presently available—inexpensively calculated through it. The establishment of density-functional perturbation theory (DFPT) [5] has considerably widened the scope of DFT, by allowing for the calculation of properties that can be expressed in terms of static response functions, as well as of vibrational excitations in the harmonic Born–Oppenheimer approximation [6]. Thanks to these advances, it is now possible to predict the infrared, Raman and inelastic neutron- or x-ray-diffraction spectra of materials with an accuracy that may be comparable with that achieved in the laboratory. Such an accuracy and flexibility open the way to the systematic use of *computational spectroscopy* as a powerful tool for characterization: by comparing the dependence of the spectral features of a system on its atomic structure—which is readily simulated on a computer—with the spectra obtained in the laboratory, it is often possible to gain detailed structural and functional information at the nanoscale, which would not be accessible by experimental means alone.

The situation is not as favorable for those spectroscopies such as absorption in the visible and UV regions, or photoemission spectroscopy, for which the excitation of electrons across the optical gap plays an essential role. Extending the scope of DFT to dynamical processes [7], so as to encompass electronic excitations is a very active field of research [8]. The resulting *time-dependent density-functional theory* (TDDFT) holds the promise to become an accurate and relatively inexpensive path to the simulation of optical spectra in molecular and nanostructured systems, but several practical and conceptual difficulties still hinder its deployment as a routine simulation tool. Many-body perturbation theory (MBPT) [9], on the other hand, provides a systematic approach to electronic excited states, but the numerical complexity of even the most basic of its approximations, such as the GW one [9–12], is such as to restrict its applicability to models of a few handfuls of inequivalent atoms, at most, these days.

The main numerical bottleneck that plagues numerical simulations within both TDDFT and, even more severely, MBPT is the occurrence of extensive sums over *virtual* (i.e. unoccupied) one-electron states in different crucial steps of both methods. It turns out that such sums can be formally expressed as matrix elements of one-electron Green's functions (in MBPT) or of the resolvent of the quantum Liouvillian

operator (in TDDFT). The recursion method of Haydock, Heine and Kelly [13–16] provides an elegant and extremely effective way of calculating such matrix elements, when they are *diagonal* and referring to *Hermitian* operators (such as quantum-mechanical Hamiltonians). Building on our recent work on TDDFT [17, 18] and on MBPT [19, 20], in this paper we extend this method to the case of general *off-diagonal* elements of the resolvent of general *non-Hermitian* operators, such as those occurring in TDDFT and MBPT, and demonstrate the resulting algorithm with a couple of paradigmatic test cases on the caffeine molecule.

1. The recursion method of Haydock, Heine and Kelly

Suppose one is interested in the calculation of some diagonal matrix element of the resolvent of a linear, Hermitian, operator H:

$$g_v(\omega) = (v, (\omega - H)^{-1} v), \tag{1}$$

where v is an arbitrary normalized vector. Following Lanczos [21], we define a chain of vectors from the three-term recursion:

$$\begin{aligned} \beta_0 q_0 &= 0 \\ q_1 &= v \\ \alpha_n &= (q_n, H q_n) \\ \beta_{n+1} q_{n+1} &= (H - \alpha_n) q_n - \beta_n q_{n-1}, \end{aligned} \tag{2}$$

where β_{n+1} is determined by imposing the normalization of q_{n+1}. The vectors generated by the recursion of equations (2) have two fundamental properties that lie at the basis of the power of Lanczos-related methods: (i) they are orthogonal (when generated in exact arithmetics) and (ii) the representation of the operator H in the basis generated by them is tridiagonal.

Let us define

$$Q_M = [q_1, q_2, \ldots q_M] \tag{3}$$

as the $N \times M$ matrix whose columns are the first M Lanczos vectors generated by the recursion of equations (2) (N is the dimension of the Hilbert space on which H is defined):

$$S_M = \begin{pmatrix} \alpha_1 & \beta_2 & 0 & \cdots & 0 \\ \beta_2 & \alpha_2 & \beta_3 & \ddots & \vdots \\ 0 & \beta_2 & \ddots & \ddots & 0 \\ \vdots & \ddots & \ddots & \alpha_{M-1} & \beta_M \\ 0 & \cdots & 0 & \beta_M & \alpha_M \end{pmatrix} \tag{4}$$

as the $M \times M$ symmetric tridiagonal matrix built with the α and β coefficients generated by the Lanczos recursion and I_M as the $M \times M$ identity matrix. The following relations hold:

$$Q_M^\top Q_M = I_M, \tag{5}$$

$$H Q_M = Q_M S_M + \beta_{M+1} q_{M+1} e_M^\top, \tag{6}$$

where $e_M^\top = [0, \cdots 1]$ is a $1 \times M$ unit array. Here and in the following we indicate matrix transposition with the '$\top$' symbol, and vectors of the Lanczos chain are treated as $N \times 1$ ('*column*') arrays. Let us now subtract ωQ_M from both sides of equation (6) and multiply the resulting equation by $q_1^\top (\omega - H)^{-1}$ on the left and by $(\omega - S_M)^{-1} e_1$ on the right, where $e_1 = [1, 0 \cdots]$ is an $M \times 1$ unit array. The resulting equation is

$$\begin{aligned} q_1^\top Q_M (\omega - S_M)^{-1} e_1 = q_1^\top (\omega - H)^{-1} Q_M e_1 \\ - \beta_{M+1} q_1^\top (\omega - H)^{-1} q_{M+1} e_M^\top (\omega - S_M)^{-1} e_1. \end{aligned} \tag{7}$$

We now use the identities

$$q_1^\top Q_M = e_1^\top \tag{8}$$

$$Q_M e_1 = q_1. \tag{9}$$

By inserting the relations equations (8) and (9) into (7) we finally obtain

$$g_v(\omega) = [(\omega - S_M)^{-1}]_{11} + \epsilon_M(\omega), \tag{10}$$

where

$$[(\omega - S_M)^{-1}]_{11} = \cfrac{1}{\omega - \alpha_1 + \cfrac{\beta_2^2}{\omega - \alpha_2 + \cdots}}, \tag{11}$$

and

$$\epsilon_M(\omega) = -\beta_{M+1} (q_1, (\omega - H)^{-1} q_{M+1}) [(\omega - S_M)^{-1}]_{M1} \tag{12}$$

is the so-called *remainder*. By neglecting the remainder in equation (10), we arrive at the celebrated continued-fraction expression for the diagonal matrix elements of the Green's function by Haydock, Heine and Kelly [13–16].

1.1. Non-diagonal matrix elements

It has long been believed that the calculation of off-diagonal matrix elements via the Lanczos method would require expressing them in terms of four auxiliary diagonal matrix elements [16]. A careful inspection of the procedure outlined above shows that, although no elegant continued-fraction expression such as in equation (11) can be found for off-diagonal matrix elements, the bulk of the numerical work done for calculating *one diagonal* matrix element, actually allows for the calculation of *many off-diagonal* matrix elements at essentially the same computational cost.

Suppose one is interested in the calculation of the off-diagonal matrix element:

$$g_{uv}(\omega) = (u, (\omega - H)^{-1} v). \tag{13}$$

By starting a Lanczos chain with $q_1 = v$ ($q_1 = u$ would also do) and following essentially the same procedure as above, g_{uv} can be expressed as

$$g_{uv}(\omega) \approx (\zeta_M, (\omega - S_M)^{-1} e_1) \tag{14}$$

where

$$\zeta_M = Q_M^\top u \tag{15}$$

is an array of dimension M (the length of the Lanczos chain) and a remainder analogous to equation (12) is neglected. Although equation (14) does not lend itself to a simple continued-fraction expression, its calculation actually only requires the solution of a tridiagonal linear system whose dimension is the length of the Lanczos chain, a task that can be accomplished with a very limited numerical effort. A crucial feature of the present algorithm that makes it convenient in practice is that the components of the ζ_M array, $\zeta_{M,i} = (q_i, u)$, can be calculated on the fly, without any need to store and retrieve all the vectors of the Lanczos chain.

1.2. Non-Hermitian operators

The generalization to non-Hermitian operators is straightforward in principle, although possibly tricky in practice. Let us assume that the matrix/operator H in equation (13) is replaced by a non-Hermitian one, L. Given a pair of vectors, q_1 and p_1 normalized by the condition $(p_1, q_1) = 1$ (although not strictly necessary, we assume both vectors to coincide with v), a chain of vector pairs can be generated through the following recursion, known as the *Lanczos bi-orthogonalization algorithm* [22]:

$$\begin{aligned} \gamma_1 q_0 = \beta_1 p_0 = 0 \\ q_1 = p_1 = v \\ \beta_{n+1} q_{n+1} = L q_n - \alpha_n q_n - \gamma_n q_{n-1} \\ \gamma_{n+1} p_{n+1} = L^\top p_n - \alpha_n p_n - \beta_n p_{n-1}, \end{aligned} \tag{16}$$

where

$$\alpha_n = (p_n, L q_n),$$

and β_{n+1} and γ_{n+1} are scaling factors for the newly generated q and p vectors, chosen so as to enforce bi-normalization:

$$(q_n, p_n) = 1.$$

In exact arithmetics, it is known that these two sequences of vectors are bi-orthogonal, i.e. $(q_n, p_m) = \delta_{nm}$, where δ_{nm} is the Kronecker symbol. The resulting algorithm is described in detail, for example, in [22]. Let us define the $(N \times M)$ matrix Q_M as in equation (3) and P_M analogously in terms of the ps instead of the qs. The following Lanczos factorization holds in terms of the quantities calculated from the recursions equations (16):

$$L Q_M = Q_M T_M + \beta_{M+1} q_{M+1} e_M^\top, \tag{17}$$

$$L^\top P_M = P_M T_M^\top + \gamma_{M+1} p_{M+1} e_M^\top, \tag{18}$$

$$P_M^\top Q_M = I_M, \tag{19}$$

where T_M is the $(M \times M)$ tridiagonal matrix:

$$T_M = \begin{pmatrix} \alpha_1 & \gamma_2 & 0 & \cdots & 0 \\ \beta_2 & \alpha_2 & \gamma_3 & 0 & \vdots \\ 0 & \gamma_3 & \alpha_3 & \ddots & 0 \\ \vdots & 0 & \ddots & \ddots & \gamma_M \\ 0 & \cdots & 0 & \beta_M & \alpha_M \end{pmatrix}. \tag{20}$$

Let us now rewrite equation (17) as

$$(\omega - L) Q_M = Q_M (\omega - T_M) - \beta_{M+1} q_{M+1} e_M^\top. \tag{21}$$

By multiplying equation (21) by $u^\top (\omega - L)^{-1}$ on the left and by $(\omega - T_M)^{-1} e_1$ on the right, we obtain

$$\begin{aligned} u^\top Q_M (\omega - T_M)^{-1} e_1 = u^\top (\omega - L)^{-1} Q_M e_1 \\ - \beta_{M+1} u^\top (\omega - L)^{-1} q_{M+1} e_M^\top (\omega - T_M)^{-1} e_1. \end{aligned} \tag{22}$$

Taking the relation $Q_M e_1 = q_1 \doteq v$ into account, equation (22) can be cast as

$$\begin{aligned} g_{uv}(\omega) &= (u, (\omega - H)^{-1} v) \\ &= (\zeta_M, (\omega - T_M)^{-1} e_1) + \varepsilon_M(\omega), \end{aligned} \tag{23}$$

where ζ_M is defined as in equation (15) and

$$\varepsilon_M(\omega) = -\beta_{M+1} (u, (\omega - L)^{-1} q_{M+1}) [(\omega - T_M)^{-1}]_{M1} \tag{24}$$

is the error made when truncating the Lanczos chain at the Mth step. Neglecting $\varepsilon_M(\omega)$ we arrive at the following approximation for $g_{uv}(\omega)$:

$$g_{uv}(\omega) \approx (\zeta_M, (\omega - T_M)^{-1} e_1), \tag{25}$$

in full analogy to the Hermitian case, expressed by equation (14). The size of the error term ε_M in equation (24) generally decreases with increasing the number M of steps in the Lanczos chain. Although the convergence of off-diagonal matrix elements may be slower than that of diagonal ones (more so near a resonance and/or in the non-Hermitian case), a manageable number of Lanczos steps is found to be sufficient to achieve the accuracy needed for spectroscopic applications, as demonstrated by the numerical applications discussed in the following sections and illustrated in figures 2, 4 and 6.

2. Time-dependent density-functional perturbation theory

The time-dependent density-functional theory of Runge and Gross [7, 8] allows for the calculation of the dynamical susceptibility of a system of interacting electrons without recourse to the explicit calculation of any excited states. Instead, excited-state energies and oscillator strengths can be estimated within TDDFT by inspecting the analytic properties of the susceptibility thus calculated. In order to find an expression for the dipole susceptibility of a system, it is convenient to start by casting the Kohn–Sham (KS) time-dependent equations of Runge and Gross [7, 8] into an operator equation for the one-electron density matrix, $\hat{\rho}(t)$:

$$\mathrm{i} \frac{\mathrm{d}\hat{\rho}(t)}{\mathrm{d}t} = [\hat{H}_{\mathrm{KS}}(t), \hat{\rho}(t)], \tag{26}$$

where

$$\hat{H}_{\mathrm{KS}}(t) = -\frac{1}{2} \frac{\partial^2}{\partial \mathbf{r}} + v_{\mathrm{ext}}(\mathbf{r}, t) + v_{\mathrm{HXC}}(\mathbf{r}, t) \tag{27}$$

is a time-dependent KS Hamiltonian, $v_{\mathrm{ext}}(\mathbf{r}, t)$ and $v_{\mathrm{HXC}}(\mathbf{r}, t)$ being the time-dependent external and Hartree plus exchange–correlation (XC) potentials, respectively, and the square

brackets indicate a commutator. In the above equation, as well as in the following, quantum-mechanical operators are denoted by a hat, '^', and Hartree atomic units ($\hbar = m = e = 1$) are used. When no confusion can arise, local operators, such as one-electron potentials, $\hat{V}$, will be indicated by the diagonal of their real-space representation, $v(\mathbf{r})$, as in equation (27). Linearization of equation (26) with respect to the external perturbation leads to

$$\mathrm{i}\frac{\mathrm{d}\hat{\rho}'(t)}{\mathrm{d}t} = [\hat{H}^{\circ}_{\mathrm{KS}}, \hat{\rho}'(t)] + [\hat{V}'_{\mathrm{HXC}}(t), \hat{\rho}^{\circ}] + [\hat{V}'_{\mathrm{ext}}(t), \hat{\rho}^{\circ}], \quad (28)$$

where $\hat{\rho}^{\circ}$ is the unperturbed density matrix, $\hat{\rho}'(t) = \hat{\rho}(t) - \hat{\rho}^{\circ}$, $\hat{V}'_{\mathrm{ext}}$ is the perturbing external potential and $\hat{V}'_{\mathrm{HXC}}$ is the variation of the Hartree plus XC potential linearly induced by $n'(\mathbf{r}, t) = \rho'(\mathbf{r}, \mathbf{r}; t)$. In the adiabatic approximation one has

$$v'_{\mathrm{HXC}}(\mathbf{r}, t) = \int \kappa(\mathbf{r}, \mathbf{r}') n'(\mathbf{r}', t)\, \mathrm{d}\mathbf{r}', \quad (29)$$

where $\kappa(\mathbf{r}, \mathbf{r}') = \frac{1}{|\mathbf{r}-\mathbf{r}'|} + \frac{\delta v_{\mathrm{XC}}(\mathbf{r})}{\delta n(\mathbf{r}')}|_{n(\mathbf{r})=n^{\circ}(\mathbf{r})}$. By inserting equation (29) into (28), one sees that the linearized Liouville equation can be cast into the form:

$$\mathrm{i}\frac{\mathrm{d}\hat{\rho}'(t)}{\mathrm{d}t} = \mathcal{L} \cdot \hat{\rho}'(t) + [\hat{V}'_{\mathrm{ext}}(t), \hat{\rho}^{\circ}], \quad (30)$$

where the action of the *Liouvillian super-operator*, $\mathcal{L}$, onto $\hat{\rho}'$, $\mathcal{L} \cdot \hat{\rho}'$, is defined as

$$\mathcal{L} \cdot \hat{\rho}' \doteq [\hat{H}^{\circ}_{\mathrm{KS}}, \hat{\rho}'] + [\hat{V}'_{\mathrm{HXC}}[\hat{\rho}'], \hat{\rho}^{\circ}], \quad (31)$$

and $\hat{V}'_{\mathrm{HXC}}[\hat{\rho}']$ is the linear operator functional of $\hat{\rho}'$ whose (diagonal) kernel is given by equation (29). By Fourier-analyzing equation (30) we obtain

$$(\omega - \mathcal{L}) \cdot \tilde{\rho}'(\omega) = [\tilde{V}'_{\mathrm{ext}}(\omega), \hat{\rho}^{\circ}]. \quad (32)$$

The expectation value of any one-electron operator can be expressed as the trace of its product with the one-electron density matrix. The Fourier transform of the dipole linearly induced by the perturbing potential, $\hat{V}'_{\mathrm{ext}}$, for example, is therefore

$$\mathbf{d}(\omega) = \mathrm{Tr}(\hat{\mathbf{r}}\tilde{\rho}'(\omega)), \quad (33)$$

where $\hat{\mathbf{r}}$ is the quantum-mechanical position operator and $\hat{\rho}'$ is the solution of equation (32). Let us now suppose that the external perturbation is a homogeneous electric field:

$$\tilde{v}'_{\mathrm{ext}}(\mathbf{r}, \omega) = -\mathbf{E}(\omega) \cdot \mathbf{r}. \quad (34)$$

The dipole given by equation (33) is therefore

$$d_i(\omega) = \sum_j \alpha_{ij}(\omega) E_j(\omega), \quad (35)$$

where the dynamical polarizability, $\alpha_{ij}(\omega)$, is defined by

$$\alpha_{ij}(\omega) = -\mathrm{Tr}(\hat{r}_i(\omega - \mathcal{L})^{-1} \cdot [\hat{r}_j, \hat{\rho}^{\circ}]). \quad (36)$$

Traces of products of operators can be seen as scalar products defined on the linear space of quantum-mechanical operators. Equation (36) can therefore be formally written as

$$\alpha_{ij}(\omega) = -\left\langle \hat{r}_i | (\omega - \mathcal{L})^{-1} \cdot \hat{s}_j \right\rangle, \quad (37)$$

where

$$\hat{s}_j = [\hat{r}_j, \hat{\rho}^{\circ}] \quad (38)$$

is the commutator between the position operator and the unperturbed one-electron density matrix. The results obtained so far and embodied in equation (37) can be summarized by saying that *within TDDFT the dynamical polarizability can be expressed as an appropriate off-diagonal matrix element of the resolvent of the Liouvillian super-operator*.

2.1. The DFPT representation

The calculation of the polarizability using equations (36) or (37) follows the algorithm explained in detail in [17, 24, 18, 25]. In particular, at variance with most current implementations and applications of TDDFT [8], we avoid the representation of the density matrix response in terms of virtual KS states. Instead, we replace the sum over virtual orbitals with projectors that can be conveniently expressed in terms of the occupied manifold only. Such a representation of response functions has been pioneered in DFPT [5, 6] and is here extended to the dynamical regime. For the purposes of the present paper, suffice it to say that the response density matrix is represented by two sets of response orbitals. Each one of these sets contains the same number of orbitals as the occupied manifold, and is kept orthogonal to the ground-state KS orbitals during the Lanczos iterations. The application of the Liouvillian super-operator $\mathcal{L}$ to each set of response orbitals amounts to the application of the unperturbed Hamiltonian to every orbital of the set followed by the real-space calculation of the response charges and the computation of $\hat{V}'_{\mathrm{HXC}}$. We conclude that each step of the TDDFT Lanczos chain costs essentially twice the price of a single step of the iterative diagonalization of the ground-state KS Hamiltonian, a single step of *ab initio* molecular dynamics or a single step of static (time-independent) DFPT. Because of these analogies, and of the crucial role played by the DFPT representation of response density matrices, we name our approach *time-dependent density-functional perturbation theory* (TDDFPT).

2.2. Lanczos extrapolation

Numerical practice has shown that obtaining a well-converged spectrum in a plane-wave (PW) implementation of TDDFT may require a few thousand (2–4000) Lanczos steps and that such a number depends on the PW kinetic-energy cutoff. However, it has also been observed that the components of the ζ_M array rapidly tend to zero in a few hundred steps, whereas the calculated Lanczos coefficients[5] (β_n and γ_n) oscillate around a value that is very close to the width of the optical spectrum (in a PW calculation this is, in turn, roughly twice the kinetic-energy cutoff). This observation opens the way to a simple, yet very effective, way of extrapolating the Lanczos recursion by using very large tridiagonal matrices when solving the linear system in equation (25) (say, $M =$

[5] The particular *symplectic* structure of the TDDFT equations [23] can be used to define a representation where the α coefficients vanish identically. The β and γ coefficients can be made to coincide except for exceptional Lanczos iterations where they have equal magnitude, but opposite sign.

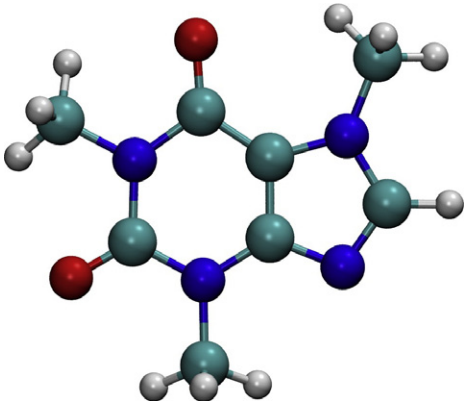

Figure 1. (Colour online) Structure of the caffeine molecule, $C_8N_4O_2H_{10}$. Blue atoms are nitrogen, red oxygen, greenish carbon and light gray hydrogen.

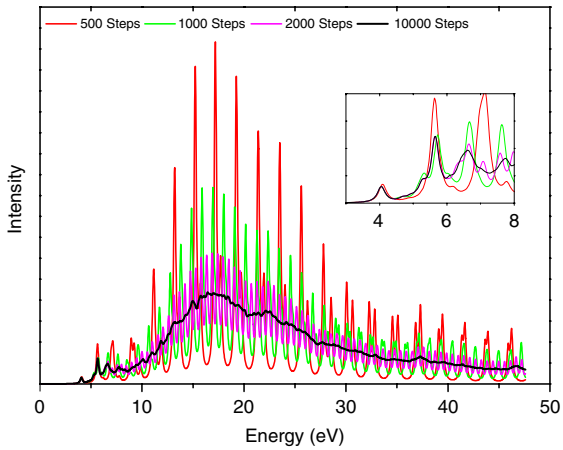

Figure 2. Absorption spectrum of the caffeine molecule calculated using our Lanczos scheme, using recursion chains of different lengths. The inset shows a magnification of the low-frequency portion of the spectrum.

10 000) and setting the components of $\zeta_{M,n} = 0$ and the Lanczos coefficients $\beta_n = \bar{\beta}$ for $n > M^\star$, where $M^\star$ is a rather small number, of the order of a few hundred (see footnote 5).

2.3. An example

The theory described above has been implemented [18] in a module of the Quantum Espresso distribution of codes for the simulation of matter based on electronic-structure theory, using DFT, pseudopotentials (PPs, norm-conserving and ultra-soft) and PWs [26]. As a demonstration of our methodology, we have calculated the absorption spectrum of the (isolated) caffeine molecule whose structure is depicted in figure 1[6].

In figure 2 we show the absorption spectrum of the caffeine molecule, as calculated by TDDFPT, using Lanczos chains of different lengths. While the main features of the spectrum (particularly at low frequency) converge rather fast, its overall appearance at intermediate and high frequency is spoiled by the inability of pseudo-discrete states resulting from the early truncation of the Lanczos chain to properly mimic a continuous spectrum. When the number of recursions is sufficiently large, these pseudo-discrete states eventually merge into a well-converged continuous spectrum.

In figure 3 we display the sequence of β coefficients calculated by our Lanczos recursion for the caffeine molecule (see footnote 5). One notices that these values are scattered around two distinct constants for odd and even iteration counts, whose average nicely approximates these two constants nicely approximates as $\frac{1}{2}$ of the kinetic-energy cutoff of the PW basis set ($E_{\rm cut} = 25$ Ryd), and that their difference approximates the position of the first optical transition at $\sim$4 eV $= 0.29$ Ryd. This fact was found and explained in [18] and can be used as a basis for extrapolating very long Lanczos chains from a few iterations, as explained in section 2.2.

[6] TDDFPT calculations were performed using the PBE [27] XC energy functional, pseudopotentials `H.pbe-rrkjus.UPF`, `C.pbe-rrkjus.UPF`, `N.pbe-rrkjus.UPF` and `O.pbe-rrkjus.UPF` from the Quantum Espresso distribution, and a PW energy cutoff of 25 and 250 Ryd for wavefunctions and the charge density, respectively. The spectra were calculated at the theoretical optimized molecular geometry, whose bond lengths deviate from experiment by <1% on average (maximum deviation <3%).

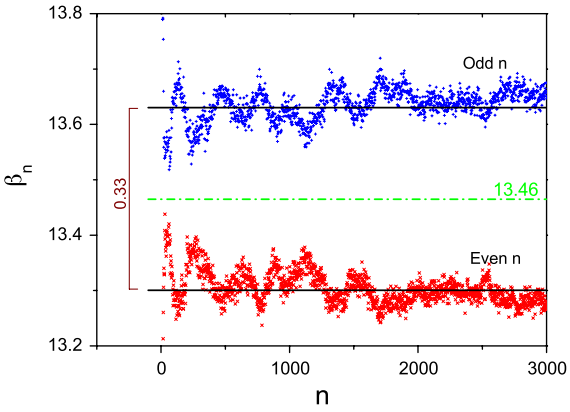

Figure 3. Coefficients of the Lanczos chain generated for the dynamic polarizability of the caffeine molecule, equation (36), calculated using the method of section 1.2, as functions of the iteration count. The green horizontal line indicates the average of the coefficients, while the vertical bar indicates the difference between the averages performed over even and odd iterations, separately.

In figure 4 we display the TDDFPT absorption spectrum of the caffeine molecule, as calculated by extrapolating the Lanczos chains following the discussion of section 2.2. The convergence of the Lanczos recursion is dramatically enhanced by chain extrapolation, allowing us to obtain a converged spectrum with as few as 500–1000 iterations.

3. Quasi-particle spectra in the GW approximation

The most elementary electronic excitation process in a molecule or in a solid is the removal/addition of an electron from a system originally in its ground state. These processes are accessible to direct/inverse photoemission spectroscopies and can be described theoretically in terms of *quasi-particle* (QP) states [9]. The QP energies E_n are eigenvalues of a Schrödinger-like equation for the so-called QP amplitudes ψ_n:

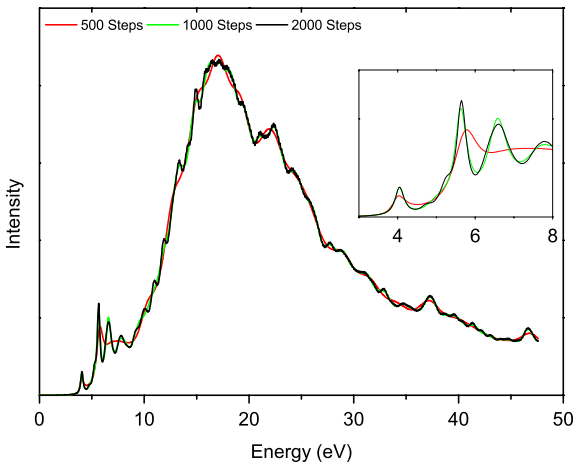

Figure 4. Absorption spectrum of the caffeine molecule calculated using our Lanczos scheme, using recursion chains of different lengths and extrapolating the calculated chain up to 10 000 steps, as described in section 2.2. The inset shows a magnification of the low-frequency portion of the spectrum.

$$\left[-\frac{1}{2}\frac{\partial^2}{\partial \mathbf{r}^2} + v_{\rm ext}(\mathbf{r}) + v_{\rm H}(\mathbf{r})\right]\psi_n(\mathbf{r}) + \int {\rm d}\mathbf{r}'\, \Sigma(\mathbf{r},\mathbf{r}';E_n)\psi_n(\mathbf{r}') = E_n\psi_n(\mathbf{r}), \tag{39}$$

where $v_{\rm H}$ is the Hartree potential and $\Sigma(\mathbf{r},\mathbf{r}',\omega)$ is the kernel of the energy-dependent and non-Hermitian self-energy operator. Equation (39) is similar to the KS equation with the XC potential replaced by the self-energy operator. In the GW approximation [10, 11] the self-energy kernel is the frequency convolution of the one-electron propagator, G, and of the dynamically screened interaction, W:

$$\Sigma_{\rm GW}(\mathbf{r},\mathbf{r}';\omega) = \frac{\rm i}{2\pi}\int_{-\infty}^{\infty} {\rm d}\omega'\, G(\mathbf{r},\mathbf{r}';\omega')W(\mathbf{r},\mathbf{r}';\omega-\omega'), \tag{40}$$

where $W = v + v\cdot\Pi\cdot v$, $\Pi(\mathbf{r},\mathbf{r}';\omega) = (1 - P\cdot v)^{-1}\cdot P$ is the *reducible polarizability*, P its *irreducible* counterpart, $v(\mathbf{r},\mathbf{r}') = \frac{1}{|\mathbf{r}-\mathbf{r}'|}$ is the bare Coulomb interaction and a dot indicates the product of two kernels, such as in $v\cdot\Pi(\mathbf{r},\mathbf{r}',\omega) = \int {\rm d}\mathbf{r}''\, v(\mathbf{r},\mathbf{r}'')\Pi(\mathbf{r}'',\mathbf{r}';\omega)$. We assume time-reversal invariance to hold—so that wavefunctions are real—and we work on the imaginary-frequency axis [28]: real-frequency results can then be recovered upon analytic continuation. At the lowest order of approximation (usually referred to as the G°W° approximation) the one-electron propagator G and the screened interaction W in equation (40) are calculated directly from the KS energies ϵ_n and wavefunctions ψ°. In particular, W is obtained from the irreducible polarizability P which is calculated in the random-phase approximation (RPA):

$$P^\circ(\mathbf{r},\mathbf{r}';{\rm i}\omega) = 4{\rm Re}\sum_{cv}\frac{\psi_c^\circ(\mathbf{r})\psi_v^\circ(\mathbf{r}')\psi_v^\circ(\mathbf{r})\psi_c^\circ(\mathbf{r}')}{{\rm i}\omega - (\epsilon_c - \epsilon_v)}. \tag{41}$$

By treating the difference between $\hat\Sigma_{\rm G^\circ W^\circ}$ and $V_{\rm XC}$ in first-order perturbation theory, QP energies are given by the nonlinear equation

$$E_n \approx \epsilon_n + \langle\psi_n^\circ|\hat\Sigma_{G^\circ W^\circ}(E_n)|\psi_n^\circ\rangle - \langle\psi_n^\circ|\hat V_{\rm XC}|\psi_n^\circ\rangle. \tag{42}$$

In [19], it was shown that it is possible to represent the polarizability operators Π and P in terms of a reduced, yet controllable accurate, orthonormal basis set $\{\Phi_\mu(\mathbf{r})\}$ built in terms of localized Wannier-like orbitals:

$$P^\circ(\mathbf{r},\mathbf{r}',{\rm i}\omega) = \sum_{\mu\nu} P^\circ_{\mu\nu}({\rm i}\omega)\Phi_\mu(\mathbf{r})\Phi_\nu(\mathbf{r}'). \tag{43}$$

Using the RPA, equation (41), $P^\circ_{\mu\nu}({\rm i}\omega)$ is

$$P^\circ_{\mu\nu}({\rm i}\omega) = -4\,{\rm Re}\sum_{v,c}\frac{1}{\epsilon_c - \epsilon_v + {\rm i}\omega} \times \int {\rm d}\mathbf{r}\,{\rm d}\mathbf{r}'\,\Phi_\mu(\mathbf{r})\psi_v^\circ(\mathbf{r})\psi_c^\circ(\mathbf{r})\psi_v^\circ(\mathbf{r}')\psi_c^\circ(\mathbf{r}')\Phi_\nu(\mathbf{r}'). \tag{44}$$

While the availability of such an optimal representation for the polarizability substantially reduces the numerical load for the calculation of the self-energy matrix elements, the number of virtual states to be included in equations (41) or (44) in order to obtain an acceptable convergence is very large, a fact often overlooked in the literature. In practice, rather accurate results are obtained by extrapolating QP energies as functions of the largest virtual-state energy included in the calculation of the irreducible polarizability, $E^\star$ (the leading error in the truncated sum decreases as the inverse of $E^\star$). The sum over empty states in equation (44) and unwieldy extrapolations of the results can be eliminated altogether by introducing the projector operator over the virtual-state (*electron*) manifold, $\hat Q_{\rm e} = \hat 1 - \hat Q_{\rm h}$, $\hat Q_{\rm h}$ being the projector onto occupied (*hole*) states [20]. In terms of $\hat Q_{\rm e}$ equation (44) is

$$P^\circ_{\mu\nu}({\rm i}\omega) = -4\,{\rm Re}\sum_v\langle\psi_v^\circ\Phi_\mu|\hat Q_{\rm e}(\hat H^\circ - \epsilon_v + {\rm i}\omega)^{-1}\hat Q_{\rm e}|\psi_v^\circ\Phi_\nu\rangle, \tag{45}$$

where

$$\langle\mathbf{r}|\psi_v^\circ\Phi_\nu\rangle = \psi_v^\circ(\mathbf{r})\Phi_\nu(\mathbf{r}). \tag{46}$$

A direct approach to equation (45) would require the inversion of $(\hat H^\circ - \epsilon_v + {\rm i}\omega)$ for every value of the (imaginary) frequency and the application of the resulting inverse to $N_{\rm v}\times N_{\rm P}$ states, where $N_{\rm v}$ and $N_{\rm P}$ are the number of valence states and polarizability basis functions, respectively, thus making the resulting algorithm awkward. In order to substantially reduce the computational load we first reduce the number of functions to which the inverse shifted Hamiltonian in equation (45) has to be applied. The first step is to set up an optimally reduced orthonormal representation for the linear space spanned by the vectors, $\{\hat Q_{\rm e}|\psi_v\Phi_\nu\rangle\}$:

$$\langle\mathbf{r}|\hat Q_{\rm e}|\psi_v^\circ\Phi_\mu\rangle \approx \sum_\alpha t_\alpha(\mathbf{r})T_{\alpha,v\mu}, \tag{47}$$

where the basis functions $\{t_\alpha(\mathbf{r})\}$ are generated by a block Gram–Schmidt procedure with elimination of linear quasi-dependences [20] and $T_{\alpha,v\mu} = \langle t_\alpha|\hat Q_{\rm e}|\psi_v\Phi_\mu\rangle$. Using equations (47), (45) is

$$P^\circ_{\mu\nu}({\rm i}\omega) \approx -4\,{\rm Re}\sum_{v,\alpha\beta}\langle t_\alpha|(\hat H^\circ - \epsilon_v + {\rm i}\omega)^{-1}|t_\beta\rangle T_{\alpha,v\mu}T_{\beta,v\nu}. \tag{48}$$

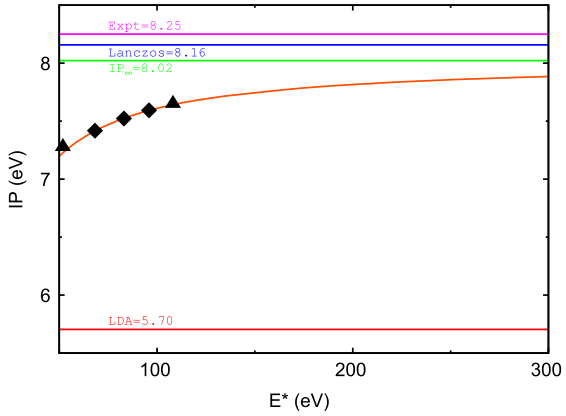

Figure 5. First (vertical) ionization potential of gas-phase caffeine, as obtained from GW calculations. Full symbols indicate results obtained by truncating the sum over virtual states in the calculation of the irreducible polarizability (see equations (41) and (44)) to the virtual energy reported on the abscissa. The data displayed as diamonds have been used to fit the results to the expression: $\mathsf{IP}(E^\star) = \mathsf{IP}_\infty - \beta/E^\star$. The resulting fit is reported in orange. The horizontal lines report the extrapolated IP, together with other relevant data (experiments from [29]).

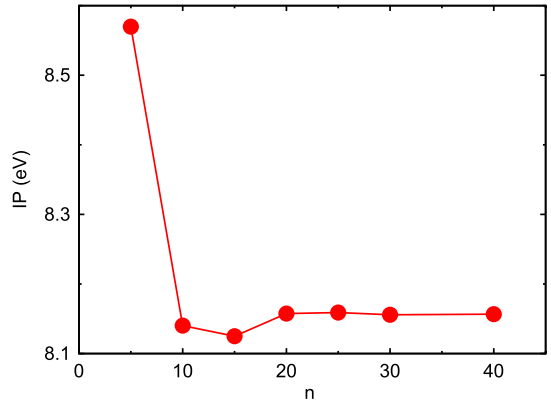

Figure 6. Convergence of the (vertical) ionization potential (IP) of gas-phase caffeine as calculated with the present GW method, as a function of the number of recursion steps, n, used in the Lanczos chain for the evaluation of the irreducible polarizability and self-energy operators.

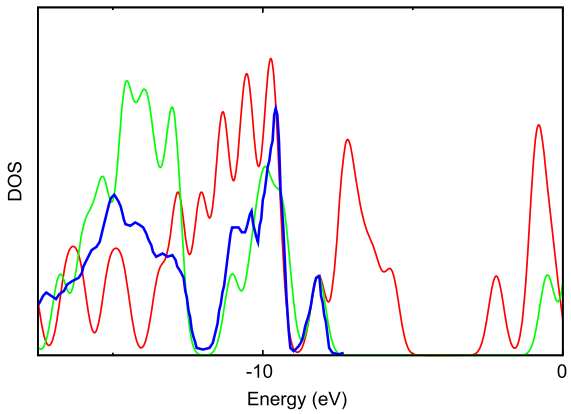

Figure 7. (Colour online) Comparison of the density of states (DOS) calculated for the caffeine molecule using the present GW method (green line) and DFT-LDA calculations (red line) with the photoemission spectrum reported in [29] (blue line). A Gaussian broadening of 0.25 eV has been used to smear the molecular lines.

Having thus reduced the number *off-diagonal* matrix elements of the resolvent of the Hamiltonian in equation (45), these matrix elements can be efficiently calculated by a Lanczos-chain algorithm, as explained in section 1.1. An analogous approach can be applied to the calculation of the expectation values of the self-energy [20]. More details on the present Lanczos-GW approach can be found in [20].

3.1. An example

The theory described above has been implemented for norm-conserving PPs [19, 20] in a module of the Quantum Espresso distribution [26]. As a demonstration of our methodology, we have calculated the QP energies of the (isolated) caffeine molecule[7].

In figure 5 we display the values of the caffeine IPs calculated using the method of [19] and limiting the sum over virtual states in the calculation of the irreducible polarizability to some specified energy range, together with the IP obtained using the present approach, as well as with DFT-LDA calculations and experiment [29]. The data reported in this figure witness the slow convergence of the sums over virtual states in equations (41) and (44) as well as the accuracy and convenience of the Lanczos method described here. Also note the great improvement of the predicted IP passing from a DFT-LDA to an MBPT-GW description of QP states.

[7] GW calculations were performed using the LDA XC functional, pseudopotentials `H.pz-vbc.UPF`, `C.pz-vbc.UPF`, `N.pz-vbc.UPF` and `O.pz-mt.UPF` from the Quantum Espresso distribution, and a PW energy cutoff of 60 and 240 Ryd for wavefunctions and the charge density, respectively. The spectra were calculated at the same geometry used in our TDDFPT calculation. The polarization basis is using the method of [19] with a conduction energy cutoff $E_c^2 = 26.15$ eV, corresponding to 750 conduction states, a cutoff on the norm of Wannier products $s_1 = 0.1$ a.u. and a cutoff on the eigenvalues of the overlap matrix between Wannier products $s_2 = 0.01$ a.u., resulting in a polarization basis of about 1320 elements.

In figure 6 we display the dependence of the caffeine IP, as calculated from the present GW method, using different numbers of Lanczos steps to calculate matrix elements of the one-electron propagator, such as in equation (48) The calculated IPs converge very rapidly as a function of the number of Lanczos steps, possibly also due to the fact that the present implementation only requires the evaluation of the relevant propagators at imaginary frequencies (hence, far from any singularities that lie on the real axis).

In figure 7 we report the density of states (DOS) of the caffeine molecule in the region of the valence energies, as calculated from the present GW method and from DFT-LDA, and compare them with a experimental photoemission spectrum from [29]. Note that no features are found in the experimental spectrum above 8.25 eV, as direct photoemission probes only valence states. Although the relative intensity of the peaks cannot be compared with experiments, due to our complete neglect of any matrix-element effects, one sees that their positions are quite well reproduced by GW, whereas LDA

shows the well-known tendency to close the QP gap (occupied states are shifted upward, whereas unoccupied one are shifted downward).

4. Conclusions

In this paper we have shown how Lanczos methods can be used to handle some of the hard numerical problems in the computer simulation of excited-state properties within TDDFT and MBPT. In the case of TDDFT, we believe that the method is close to be numerically optimal if detailed information on individual excited states is not required. Of course, no numerical advance can cope with the inadequacy of currently available XC kernels to properly describe excitonic and charge-transfer effects in the excited states. As for MBPT, the approach presented here can be easily extended to the calculation of optical spectra using the Bethe–Salpeter equation (BSE). On the other hand, a simplified version of the BSE featuring a statically screened exchange kernel has been recently treated with success using an approach similar to that used here for TDDFT [30]. All in all, we believe that the Lanczos method will allow for substantial progress in the numerical simulation of electronic excited states in the near future.

Acknowledgments

This paper is dedicated to Professor Mike Gillan on the occasion of his 65th birthday. The authors wish to thank D Rocca, A M Saitta, G Stenuit, and B Walker for collaborating with them at various stages of this work. SB would also like to thank Giuseppe Pastori Parravicini for being his early mentor and for making him aware of the existence, beauty and power of Lanczos methods.

References

[1] Hohenberg P and Kohn W 1964 *Phys. Rev.* **136** B864
[2] Kohn W and Sham L J 1965 *Phys. Rev.* **140** A1133
[3] Marzari N 2006 *MRS Bull.* **31** 681
[4] Martin R 2004 *Electronic Structure: Basic Theory and Practical Methods* (Cambridge: Cambridge University Press)
[5] Baroni S, Giannozzi P and Testa A 1987 *Phys. Rev. Lett.* **58** 1861
[6] Baroni S, de Gironcoli S, Dal Corso A and Giannozzi P 2001 *Rev. Mod. Phys.* **73** 515
[7] Runge E and Gross E K U 1984 *Phys. Rev. Lett.* **52** 997
[8] Marques M A L, Ullrich C L, Nogueira F, Rubio A, Burke K and Gross E K U 2006 *Time-Dependent Density Functional Theory* (*Lecture Notes in Physics* vol 706) (Berlin: Springer)
[9] Hedin L and Lundqvist S 1969 *Solid State Physics* vol 23, ed F Seitz, D Turnbull and H Ehrenreich (New York: Academic) p 1
[10] Hedin L 1965 *Phys. Rev.* **139** 796
[11] Hybertsen M S and Louie S G 1985 *Phys. Rev. Lett.* **55** 1418
[12] Aryasetiawan F and Gunnarsson O 1998 *Rep. Prog. Phys.* **61** 237
[13] Haydock R, Heine V and Kelly M J 1972 *J. Phys. C: Solid State Phys.* **5** 2845
[14] Haydock R, Heine V and Kelly M J 1975 *J. Phys. C: Solid State Phys.* **8** 2591
[15] Bullet D W, Haydock R, Heine V and Kelly M 1980 *Solid State Physics* vol 35, ed F Seitz, D Turnbull and H Ehrenreich (New York: Academic)
[16] Grosso G and Pastori Parravicini G 1985 *Memory Function Approaches to Stochastic Problems in Condensed Matter* (Hoboken, NJ: Wiley) chapter IV, pp 133–81
[17] Walker B, Saitta A M, Gebauer R and Baroni S 2006 *Phys. Rev. Lett.* **96** 113001
[18] Rocca D, Gebauer R, Saad Y and Baroni S 2008 *J. Chem. Phys.* **128** 154105
[19] Umari P, Stenuit G and Baroni S 2009 *Phys. Rev.* B **78** 201104
[20] Umari P, Stenuit G and Baroni S 2009 GW quasi-particle spectra from occupied states only *Phys. Rev.* B at press (arXiv:0910.0791v1 [cond-mat.mtrl-sci])
[21] Lanczos C 1950 *J. Res. Natl Bur. Stand.* **45** 255
[22] Saad Y 2003 *Iterative Methods for Sparse Linear Systems* 2nd edn (Philadelphia, CA: SIAM)
[23] Chernyak V, Schulz M, Mukamel S, Tretiak S and Tsiper E 2000 *J. Chem. Phys.* **113** 36
[24] Rocca D 2007 Time-dependent density-functional perturbation theory: new algorithms with applications to molecular spectra *SISSA PhD Thesis* http://www.sissa.it/cm/thesis/2007/Dario_Rocca_PhD_Thesis.pdf
[25] Walker B and Gebauer R 2007 *J. Chem. Phys.* **127** 164106
[26] Scandolo S *et al* 2005 *Z. Kristallogr.* **220** 574–9
Giannozzi P *et al* 2009 *J. Phys.: Condens. Matter* **21** 395502 http://www.quantum-espresso.org
[27] Perdew J P, Burke K and Ernzerhof M 1996 *Phys. Rev. Lett.* **77** 3865
[28] Rojas H N, Godby R W and Needs R J 1995 *Phys. Rev. Lett.* **74** 1827
Rieger M M, Steinbeck L, White I D, Rojas H N and Godby R W 1999 *Comput. Phys. Commun.* **117** 211
[29] Feyer V, Plekan O, Richter R, Coreno M and Prince K C 2009 *Chem. Phys.* **358** 33
[30] Rocca D, Lu D and Galli G *Phys. Rev. Lett.* in preparation